An Automated Microfluidic System for Morphological Measurement and Size-Based Sorting of *C. Elegans*

Xianke Dong, Pengfei Song, and Xinyu Liu

***Abstract*— This paper reports a vision-based automated microfluidic system for morphological measurement and size-based sorting of the nematode worm *C. elegans*. Exceeding the capabilities of conventional worm sorting microfluidic devices purely relying on passive sorting mechanisms, our system is capable of accurate measurement of the worm length/width and active sorting of worms with the desired sizes from a mixture of worms with different body sizes. This function is realized based on the combination of real-time, vision-based worm detection and sizing algorithms and automated on-chip worm manipulation. A double-layer microfluidic device with computer-controlled pneumatic valves is developed for sequential loading, trapping, vision-based sizing, and sorting of single worms. To keep the system operation robust, vision-based algorithms on detecting multi-worm loading and worm sizing failure have also been developed. We conducted sorting experiments on 319 worms and achieved an average sorting speed of 10.4 worms per minute (5.8 s/worm) with an operation success rate of 90.3%. This system will facilitate the worm biology studies where body size measurement and size-based sorting of many worms are needed.**

***Index Terms*— Microfluidics, *C. elegans*, size-based sorting, morphological measurement, image processing, automation.**

I. Introduction

THE nematode worm *C. elegans* (or simply the worm) is a tiny model organism widely used in many areas of biology, including ageing, development, neuroscience, and behavior [1]–[4]. A *C. elegans* has four distinct larval stages (L1, L2, L3, and L4) and one adult stage, which are experimentally characterized by its body size. The body size of *C. elegans*, usually measured in its length, is a basic physiological parameter, and its regulation mechanisms have been extensively studied in terms of genetic variations, signaling pathways, feeding conditions, among others [5]–[11].

In many experiments, the worm body size is typically used as a straightforward physiological marker to identify size-related phenotypes, which can then be analyzed for the potential biophysical and biochemical mechanisms regulating the worm body size. Conventionally, the body size measurement of *C. elegans* is performed either by an operator via visual inspection under an optical microscope or through off-line measurement using commercial image processing software (e.g., ImageJ and WormLab), which is time-consuming and labor-intensive. These methods are especially inconvenient to use if a large number of *C. elegans* worms need to be sorted based on their size differences for further studies.

Recently, microfluidic devices have emerged as useful tools for *C. elegans* research, and have advanced various kinds of worm biology studies [12]–[30]. Many microfluidic devices have been reported for facilitating sorting of the *C. elegans* worms at different larval stages from their mixtures based on age-dependent properties (e.g., length, locomotion, and electrotaxis behavior) of *C. elegans* [18], [19], [21]–[26]. Among these devices, several designs integrated novel microfluidic architectures, such as 'smart maze' [24], engineered pillar arrays [25], and size adjustable microfluidic channels [26] for passive size-based sorting of *C. elegans* worms at different developmental stages. These passive worm sorting methods demonstrate high-throughput sorting capabilities; however, they are all based on pure microfluidic passive sorting mechanisms and cannot accurately measure the body sizes of individual worms. Therefore, they are unsuitable for use in experiments that directly employ worm size regulation as phenotypic trait and require size quantification and size-based sorting of many worms [31], [32].

For instance, the worm length naturally varies within a range of ± 10 μm during swimming in its culture medium. The existing microfluidic devices, although capable of conducting size-based worm sorting based on certain passive fluidic mechanisms, can never detect such size variance with an accuracy of <10 μm. A commercial worm sorting instrument so called the BioSorter (Union Biometrica) is also available and capable of sorting *C. elegans* based on the worm body size measured through fluorescence imaging, but it is fairly expensive and thus not easily accessible to every worm biology laboratory. In addition, its algorithms for measuring the worm body morphology cannot be customized for specific experimental needs. Therefore, affordable and customizable platforms for

Manuscript received October 8, 2018; revised January 31, 2019; accepted February 27, 2019. Date of publication March 8, 2019; date of current version June 28, 2019. This work was supported by the National Sciences and Engineering Research Council of Canada under Grant RGPIN-2017-06374, Grant RGPAS-2017-507980, and Grant DGDND-2017-00001. The work of X. Dong and P. Song was supported by the Chinese Scholarship Council. *(Corresponding author: Xinyu Liu.)*

X. Dong and P. Song are with the Microfluidics and BioMEMS Laboratory, Department of Mechanical and Industrial Engineering, University of Toronto, Toronto, ON M5S 3G8, Canada, and also with the Department of Mechanical Engineering, McGill University, Montreal, QC H3A 0C3, Canada.

X. Liu is with the Microfluidics and BioMEMS Laboratory, Department of Mechanical and Industrial Engineering, University of Toronto, Toronto, ON M5S 3G8, Canada (e-mail: xyliu@mie.utoronto.ca).

This paper has supplementary downloadable material available at http://ieeexplore.ieee.org, provided by the author.

Digital Object Identifier 10.1109/TNB.2019.2904009

automated body size measurement and size-based sorting of *C. elegans* are still highly demanded.

This paper reports an automated microfluidic system, which combines automated microfluidic control and image processing techniques, for high-accuracy body size measurement and size-based sorting of *C. elegans* worms. A microfluidic device with computer-controlled, on-chip pneumatic valves is developed to sequentially load single worms into a worm observation chamber, and a host computer, which integrates customized image-processing algorithms and a multi-channel pressure control unit, is used to accurately measure the length and width of the worm body and coordinate the pneumatic-valve operations accordingly for automated size-based worm sorting. The system's accuracy of worm size measurement is comparable to that of commercial worm analysis software (WormLab). Proof-of-concept experiments are performed to sort young adult worms (900-1000 μm length) from a swarm of L4, young adult, and adult worms, demonstrating an average sorting speed of 10.4 worms per minute (5.8 s per worm) with a success rate of 90.3%. We also conduct typical viability tests on the sorted worms and confirm that the device does not impose adverse effects on their physiological conditions. This microfluidic system holds great potential to significantly facilitate *C. elegans* studies that use worm body size parameters as experimental readouts and need high-speed size-based worm sorting.

II. System Setup and Operation

A. System Setup

The worm sorting system, as shown in Fig. 1, was established based on an inverted microscope (IX83, Olynmpus) with a 4× objective, and a CMOS camera (acA2000-340km, Basler; 2040×1080 pixels) was used for real-time imaging (50 fps) of single worms inside the worm observation chamber of the microfluidic device. To control the pneumatic valves through regulated pressures, we developed a 16-channel pressure control unit. The pressure unit consists of a microcontroller (mega2560, Arduino), three manually-adjustable pressure regulators (ARG20-N01G1-Z, SMC Pneumatics), 16 solenoid valves (S10MM-30-24-2/A, Pneumadyne Inc.), and a circuit board with 16 transistors (2N3094) to turn on/off the valves. The camera and the pressure unit were controlled by a host computer (3.1GHz CPU, 16G RAM). Customized image processing and hardware control algorithms were implemented using C++ in Microsoft Visual Studio 2016, and the image processing algorithms were composed using OpenCV functions (version 3.4). This system can be readily established based on an optical microscope existing in any worm biology laboratory with three additional items added (i.e., the microfluidic device, the pressure control unit, and the syringe pump). Thus, our method provides a more cost-effective solution for size-based worm sorting than the commercial BioSorter.

B. Microfluidic Device Design and Fabrication

The microfluidic device consists of two microchannel layers, as shown in the blue and red in Fig. 2. The fluidic channels were arranged in the top flow layer to manipulate

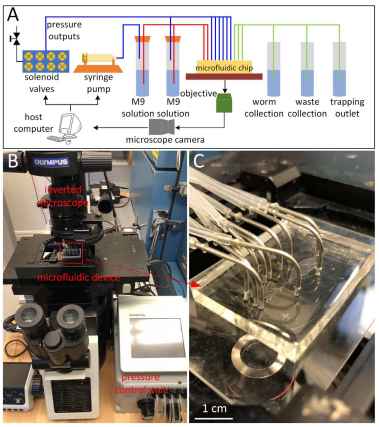

Fig. 1. Experimental setup of the worm sorting system. A: Schematic system setup. B, C: Photographs of (B) the system and (C) the microfluidic device.

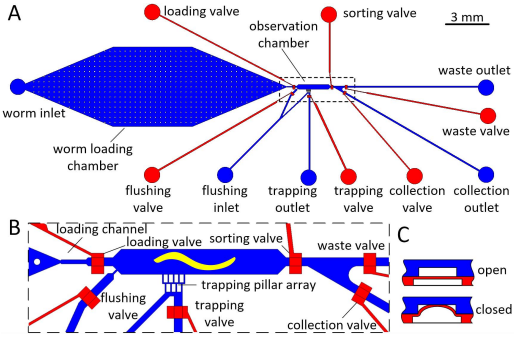

Fig. 2. Schematic of the double-layer microfluidic device. A: Microfluidic channel design. B: Details of the observation chamber. C: ON/OFF mechanism of the two-layer microfluidic system.

single worms, and the pneumatic valves were integrated in the bottom control layer. The cross-section view of a pneumatic valve is shown in Fig. 2C to illustrate its operation principle. The channel height of the top flow layer was designed to be 45 μm (approximately the average diameter of young adult worms), which confines the vertical movement of a worm during worm imaging and thus improves the accuracy of body size measurement. The microchannels in the top flow layer can be separated into three regions based on functionality: i) the loading chamber, ii) the observation chamber, and iii) the downstream sorting channels.

The worm loading chamber is a large worm storage area supported by micro-pillar arrays, as shown in Fig. 2A. For worm loading, unsynchronized *C. elegans* worms (at different developmental stages) on a culture plate are manually picked using a pipette and loaded into the worm loading inlet of the microfluidic device. During worm picking, the picked worms are sequentially transferred into multiple droplets of pure M9 solution on a clean agar plate, and this process removes large impurities from the picked worm bodies and avoids clogging of the microfluidic device with loaded worms. As a preparation step, a positive pressure of 5 psi will be applied to the device inlet to flush small impurities and worms at L1, L2, and L3 stages out of the worm loading chamber and only leave larger worms (L4, young adult, and adult stages) that are stopped by the pillars for subsequent sorting. The spacing between adjacent pillars was set to be 240 μm to reduce the loading speed of single worms and avoid device

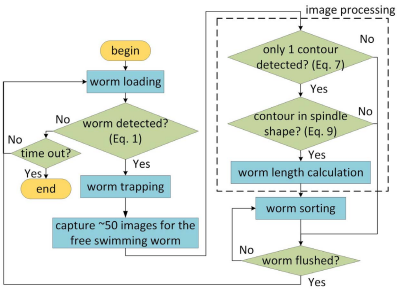

Fig. 3. Flowchart of the system operation procedure.

clogging and duble loading (two worms enter the observation chamber together) [25].

The observation chamber, with a width of 300 μm and a length of 2100 μm, was designed to contain a single worm with enough space for swimming, and the field of view (FOV) of the microscope (with a 4× objective) always covers the entire observation chamber for worm size measurement. Specifically, the entrance of the observation chamber is a 60 μm wide loading channel with a 30 μm nip at its front (Fig. 2B). The 30 μm nip of the loading channel was designed to be slightly narrower than the smallest diameter (∼35 μm) of L4 worms (the smallest among the mixture of L4, young adult and adult worms we will sort) to reduce the chance of multi-worm loading into the chamber and improve the operation success rate. In our experiments, we did not observe clogging of the nip by a single worm even for the young adult and adult worms with body widths larger than the nip width, which is mainly because of the highly deformable worm body allowing it squeeze through the nip.

As the width of the observation chamber (300 μm) is much larger than that of the loading channel (60 μm), there is a flow rate drop of the incoming fluid when it enters the observation chamber [20], which reduces the entering speed of the worm and leaves longer response time for the pneumatic micro-valves to close the observation chamber and trap the loaded worm. Note that the down stream sorting valves (waste and collection valves) are closed during worm loading, and the fluid from the loading channel will flow to the trapping outlet (Fig. 2B). Thus, the worm flushed with the fluid through the loading channel will be trapped by the trapping pillar array (pitch: 15 μm) at the junction of the trapping channel and the observation chamber. This trapping effect further lowers the speed of the worm and completely avoids any worm escape out of the observation chamber due to its high entering speed. The trapping channel and the flush channel are connected together just outside the trapping pillar array.

When the size measurement of the current worm is completed, a 20 psi pressure will be applied to the flush inlet to flush the worm out of the observation chamber for downstream sized-based sorting. The straight flow channel at the outlet side of the observation chamber is to collect the waste worms of no interest (e.g., worms with undesired sizes, multiple worms simultaneously loaded into the observation chamber, or worms with failed size measurements), for which the waste valve is opened and the collection valve is closed. If a worm is measured to have the desized size, it will be sorted to the collection channel (waste valve off and collection valve on).

The microfluidic device was fabricated from polydimethylsiloxane (PDMS) via standard multi-layer soft lithography. The mold masters of the two device layers were fabricated through photopatterning SU-8 2025 on silicon wafers. Pre-cured PDMS was prepared with base-curing agent w/w mixing ratios of 5:1 and 20:1 for molding the top flow layer and the bottom control layer, respectively. The thickness of the bottom control layer was controlled to be 40 μm by spin-coating the uncured PDMS on its mold master at 1500 rpm.

C. Operation Procedure for Automated Worm Sorting

By visually detecting/sizing individual loaded worms and regulating the valves (through the pressure unit), the system is capable of repetitively loading a single worm into the observation channel, analyze its body size parameters (length and width), and sort it based on its measured length. The sorting process (Fig. 3) consists of three operation steps: i) the loading step, ii) the trapping/sizing step, and iii) the sorting step. The corresponding on/off states of the valves and supplied pressures are shown in Table I.

At the loading step, a constant loading flow of 5 μl/s is applied to the worm loading inlet by a syringe pump (Fig. 1A) to load single worms sequentially into the observation chamber. In the meanwhile, the sorting valve and the flushing valve are closed so that the main fluidic flow through the observation chamber could travel from the loading channel, through the trapping pillar array, to the the trapping channel. As a result, once a worm is loaded into the observation chamber, it will be trapped at the trapping pillar array because of the fluidic pressure. A worm detection algorithm (see Section III-A) running continuously on the host computer detects whether the worm body has completely entered the observation chamber (which is called a 'complete loading'). When a complete loading is detected, the loading valve is closed, the loading flow is shut off, and the trapping valve remains open for an additional period of time (200 ms) to move the entering worm to the trapping pillar array. In addition, the syringe pump quickly withdraws 10 μl fluid to prevent the loading of a second worm. The back flow caused by the syringe pump releases the loaded worm from the trapping pillar array and makes the worm ready for body size measurement. The body size parameters of the worm are repeatedly measured from 50 consequent image frames by a customized image processing algorithm, and the 50 measurements were averaged to provide the final result. If the measured worm body length is within a user-specified range, the downstream waste valve is closed and the collection valve opened, and the flushing pressure is turned on to flush the worm into the collection outlet. Otherwise, the worm will be flushed into the waste outlet. Then, the whole process will start again to sort the next worm. Typically, the entire sorting process takes 5.8 s.

III. Techniques for Automated Worm Sorting

A. Worm Detection Inside the Observation Chamber

In the sorting experiments, a complete worm loading needs to be first detected to trigger the worm trapping process (by the trapping chamber) and prevent the loading of a second worm. For a worm being carried by the 5 μl/s flow through the 60 μm wide loading channel, its captured image sequence appears to

TABLE I
STATES OF THE VALVES AND SUPPLIED PRESSURES AT THREE OPERATION STEPS

System states	worm inlet	flushing pressure	loading pressure	flushing valve	trapping valve	sorting valve	waste valve	collection valve
loading	on	off	open	closed	open	closed	open	closed
trapping	off	off	closed	closed	closed	closed	open	closed
sorting	off	on	closed	open	closed	open	depending on the worm length	depending on the worm length

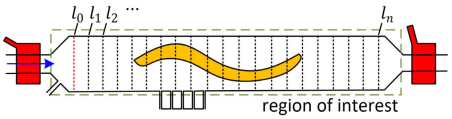

Fig. 4. Worm detection graph within the observation chamber.

be only a blurred shadow. Thus, the detection algorithm needs to be not only fast but also effective to pick up the blurred worm image.

In the worm detection algorithm, the average pixel intensity of a specific area in the observation chamber is used as a reliable indicator for the presence of a worm, since the worm body is darker than the channel background and the occupancy of an area by the worm body causes significant drop in the average pixel intensity of that area. To improve the image processing speed, we continuously measured the average intensity drops of a series of parallel lines along the chamber width (Fig. 4). The lines $l_0, l_1, ..., l_n$ evenly spread throughout the observation chamber with a pitch of d. A background C++ thread repetitively calculates the average intensity drops of the lines during real-time imaging. The worm is considered to be detected if either one of the following two criteria are satisfied.

$$\begin{cases} \exists i \in \{0, ...n\} s.t. \Delta I(\bar{l}_i) > \delta, \Delta I(\bar{l}_{i+1}) > \delta, & \Delta I(\bar{l}_0) < \delta \\ \arg\max_i \{\Delta I(\bar{l}_i) > \delta, \Delta I(\bar{l}_{i+1}) > \delta\} > \dfrac{L}{d}, & \Delta I(\bar{l}_0) \geq \delta \end{cases} \quad (1)$$

where $\Delta I(\bar{l}_i)$ is the average intensity drop of the pixels on the line l_i, δ is an experimentally determined threshold, and L is the length of a young adult worm. The first criterion indicates that a worm larger than d has been completely loaded, while the second one indicates that the body portion longer than the threshold L has been loaded. In our experiments, $d = 120$ μm and $L = 1000$ μm. Through our testing, the worm detection algorithm took less than 2 ms to process one image frame and provided a detection success rate of 100%.

B. Vision-Based Worm Size Measurement

In the trapping step, the microscope camera takes the image of the observation chamber at a frame rate of 50 fps, and the worm body size parameters are repeatedly measured for 1 s (50 consequent frames). We developed custom-made image processing algorithms for worm body size measurement so that our system could readily integrate and customize the algorithms for automated operation. To ensure system operation reliability, we adopted mature algorithms here for rapid recognition of worm body boundaries and accurate measurement of the worm size.

1) Worm Length Measurement: Before an experiment begins, a region of interest (ROI) will be selected on the live video displayed by the system control software, which covers the observation chamber. One frame of the ROI grabbed initially before worm loading is used as a background image. Once a worm image is grabbed, as illustrated in Fig. 5A, it is first subtracted by the background image to remove unnecessary features of the chamber edges and the background texture. Then, the ROI is averaged by a 3×3 *Gaussian* mask to reduce image noise and binarized using the *Otsu* method [33]. A 3×3 *erode* and *dilate* operator is applied to the resultant image, to eliminate the small debris in the image (Fig. 5B). After that, all the contours within the image are identified, and only the largest one is detected as the boundaries of the worm body (Fig. 5C).

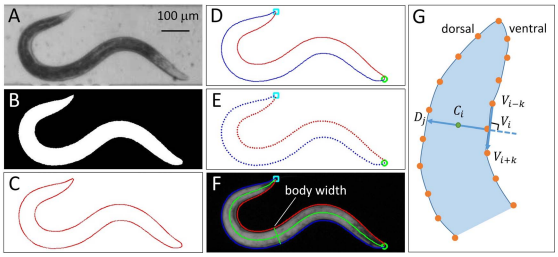

Fig. 5. Image processing algorithm for calculation of worm morphology features. A: Original image of a worm confined within the observation chamber. B: Binarized image. C: Extracted worm boundary. D: Dorsal and ventral sides of the worm on its boundary. E: Resample of the dorsal and ventral sides. F: Calculation of the centerline and the width on the worm body. G: Schematic view of the algorithm.

The obtained worm contour points are evenly re-sampled by a fixed distance with a linear interpolation method. Denoting the re-sampled points as $P_i, i = 1, ...n$, the acuity of a specific boundary point with respect to its adjacent points can be evaluated as

$$M_{k,i} = (P_{i+k} - P_i) \cdot (P_{i-k} - P_i) \doteq l_k^2 \cos\alpha_i \quad (2)$$

where k is the vector size, l_k is the vector length, α_i is the acute angle between two intersection vectors. A larger $M_{k,i}$ indicates a smaller α_i and a sharper boundary point. Thus, the worm tail can be identified by evaluating $M_{k,i}$, since it is the sharpest point on the worm body contour. However, this process is dependent on k, as a small k leads to a local optimal point while a large k leads to a biased result. To avoid this disadvantage, the large and small vector lengths are combined and the worm tail point P_t is defined by

$$t = \arg\max_i \{M_{l_1,i} + l_1^2/l_2^2 \cdot M_{l_2,i}\}, \quad i \in \{1, ...n\} \quad (3)$$

The head P_h of the worm is defined as

$$h = \arg\max_i \{M_{l_1,i} + l_1^2/l_2^2 \cdot M_{l_2,i}\}, \quad i \in \{1, ...n\} - \{t - a, ...t + a\} \quad (4)$$

where a is the region width to exclude the tail area. In experiments, we set $a = n/4, l_1 = n/40$, and $l_2 = n/100$.

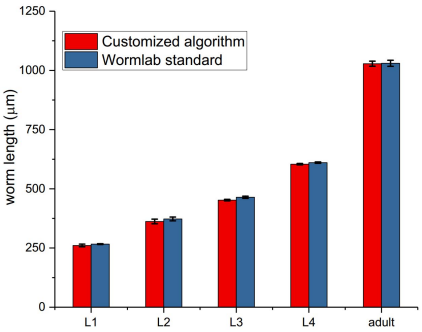

Fig. 6. Comparison of the worm sizing results from our algorithm and the WormLab software (n = 20).

After identifying the head and tail points, the contour points of the worm body can be separated to the ventral and dorsal sides, as shown in Fig. 5D. These two point sets are further re-sampled by distance through linear interpolation with a sample size of s. We get the ventral points V_i and dorsal points D_i ($i = 1, ...s$), as illustrated in Fig. 5E. Fig. 5G shows the calculation of centerline points C_i, which is defined by

$$C_i = \frac{1}{2}(V_i + D_j), \quad i = \{1, ...s\}$$

where

$$j = \arg\min_m\{(V_{i+k} - V_{i-k}) \cdot (D_m - V_i)\},$$
$$m = \{i - a, ..., i + a\}$$

and a is a parameter to limit the searching area and $a = 10$ in our experiments. With the centerline points defined, the worm length is calculated as

$$L = \sum_{i=1}^{s-1} |C_{i+1} - C_i| \tag{5}$$

In our experiments, we found $s = 100$ provided accurate measurement of the worm body length comparable to that of the commercial software WormLab. The accuracy of the length calculation can be further improved by increasing s.

2) Worm Width Measurement: Besides the worm length measurement, we also developed an algorithm for quantifying the worm body widths at different locations along its length. With the body widths measured, one can calculate the worm body volume by assuming circular cross-sections of different segments of the worm body. This worm body volume parameter could serve as an additional physiological parameter of the worm, and cannot be measured by the existing commercial software.

The width is the distance between the corresponding points on the dorsal and ventral sides, and it is distributed along the body as

$$w_i = \left|D_j - V_i\right| \tag{6}$$

where D_j and V_i have been defined in Section III-B.1. We define the width of a worm as the width in the middle point of the recognized worm body centerline ($w_{s/2}$; see Fig. 5F). The worm width data were also used for detecting calculation failures of the body size measurement algorithm (see Section III-D).

With the camera frame rate of 50 fps, between two adjacent frames the worm is not able to swim out of a distance of 20 pixels when it is confined within the observation chamber. Once the worm body in the first frame is recognized, the ROI of the next frame is reduced to the region extended from the rectangle enclosing the worm body by 20 pixels from its edges. With this much smaller ROI, the image processing time for the subsequent frames is greatly reduced. Based on our experiments, the average time required for body size analysis in each frame was 5 ms, 7 ms, 10 ms, 12 ms, 15 ms, and 17 ms for L1, L2, L3, L4, young adult, and adult worms, respectively.

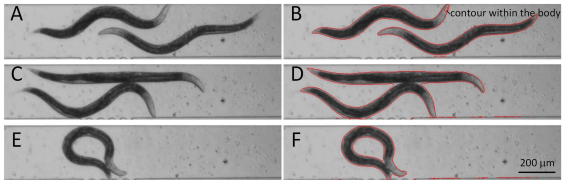

Fig. 7. Detection of multi-worm loading and calculation failure. A, C, E: Raw images illustrating cases of multi-worm loading, worm body contact, and self-coiling, respectively. B, D, F: Contour detection results that cannot be further processed by the proposed worm length measurement algorithm.

To verify the accuracy of the proposed algorithm for worm length measurement, we continuously grabbed 20 images of worms at various developmental stages, and compare the worm length data calculated by our algorithm with those from the commercial software WormLab. As shown in Fig. 6, there is no significant difference among all the 5 comparison groups for worm length measurement (average difference: 1.8%). The data measured by both our algorithm and WormLab show that the length of the same worm during locomotion vary in a range of $\sim$10 μm during its natural undulation movement. The largest standard deviation (10.8 μm) of the worm length measured by our algorithm (Fig. 6) was determined to be the measurement accuracy of our algorithm.

C. Automatic Detection of Multi-Worm Loading

If more than one worm is loaded into the observation chamber (Fig. 7A), the measurement algorithm will not work properly. Also, the microfluidic device cannot separate the simultaneously loaded worms for downstream sorting. Although the nip design of the loading channel can reduce the chance of multi-worm loading, simultaneous loading of more than one worm into the observation chamber may still happen occasionally. To this end, we designed an image processing algorithm to automatically detect the multi-worm loading. Before the worm length calculation, all the identified contours within the ROI are extracted. The largest contour and the second largest contour are denoted as $\{P\}_1$ and $\{P\}_2$, respectively. If

$$\{P\}_2 \notin \{P\}_1, \text{and } card\{P\}_2 > \lambda\ card\{P\}_1 \tag{7}$$

multi-worm loading is considered to be occurring, where $card\{P\}$ denotes the number of members in the set P. Due to non-uniform transparency of the worm body, some inner organs within the worm body may be occasionally detected as some connected regions (the small region in Fig. 7B). The first condition, $\{P\}_2 \notin \{P\}_1$, is to avoid detecting the inner organs as a separate worm. The second condition is to ensure that the size of the connected domains the algorithm detects are large enough to be a second worm contour. λ as set to be 0.25, which

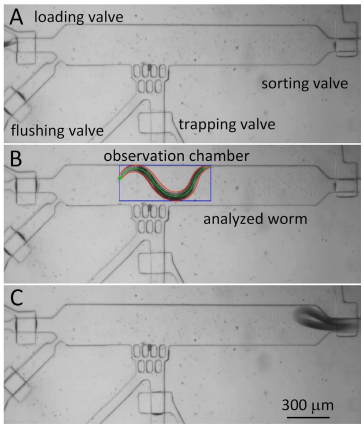

Fig. 8. Screen shots of the observation chamber and the target worm at A: the loading step; B: the body size measurement step; C: the sorting step.

is the approximate size ratio between an adult worm and an L1 worm. Fig. 7B shows two simultaneously loaded worms detected by the algorithm. Upon being detected, all the simultaneously loaded worms contained in the observation chamber are directly flushed to the waste outlet without sorting.

There are also chances that two or more worms are loaded into the chamber, and their bodies contact each other in the image. This leads to the visual recognition of a connected contour of the two worm bodies. In this case, the multi-worm loading is detected by another algorithm for calculation failure, as discussed in Section III-D.

D. Automatic Detection of Calculation Failure

During the trapping procedure, multiple worms may be loaded into the observation chamber together and the worm sizing algorithm detects their bodies to be a single connected contour (Figs. 7C and 7D). The algorithm described in Section III-C cannot detect this case. In addition, a single freely swimming worm may also display coiling behavior in some of the image frames (Fig. 7E). One region of the body contacts with other regions, causing failure of the worm body sizing algorithm (Fig. 7F). We designed another algorithm to detect both events of multi-worm loading with a connected body contour and single-worm coiling.

As discussed in [34], the width distribution along the worm body is characterized by

$$w_i = w_{s/2}(1 - e^{-0.1(s-|2i-s|)}) \tag{8}$$

To eliminate the failure calculations, the worm width is evaluated at several points along the worm centerline. Only the frames satisfying the following criteria are considered to contain a single worm feature without coiling:

$$\begin{cases} L_1 < L < L_a \\ a < L/w_{s/2} < b \\ w_i = w_{s/2}(1 - e^{-0.1(s-|2i-s|)}) + \eta w_i, \quad i = \left\{\frac{s}{8}, \ldots \frac{7s}{8}\right\} \end{cases} \tag{9}$$

L_1 and L_a are the lengths of L1 and adult worms, respectively. $L_1 = 250$ μm and $L_a = 1500$ μm were used in our experiments. The boundaries of the length-to-width ratio a and b were set to be 8 and 17. η is a false tolerance coefficient, and was set to be $-0.3 < \eta < 0.3$ in our experiments. The first and second criteria limit the length and length-to-width ratio of the calculation result, while the third criteria defines the qualified worm contour as a spindle shape as illustrated in Eq. 8. Together with the restrictions of Eq. 7, the target contour is bounded to be a signal worm within the observation channel without self-coiling, which can be further processed by our algorithm. The above criteria are applied to analyzing each image frame during the worm trapping period (∼50 frames in total), The frames violating these criteria will be neglected without worm size measurement, and the final length and width of the current worm body are calculated as the average values from all the qualified image frames.

TABLE II
WORM SORTING EXPERIMENTAL RESULTS

	Time cost for successful sorts (second)	Sorting (times)	Multi-loading (times/worms)	Calculation failure (times/worms)
Batch 1	691	139	11/23	1/3
Batch 2	196	47	7/17	1/3
Batch 3	263	41	3/10	1/2
Batch 4	168	29	1/2	1/4
Batch 5	142	23	1/3	0
Total	1460	279	23/55	4/12

TABLE III
POST-SORTING SIZE MEASUREMENT RESULTS

Size range	Collected worms (93)	Flushed worms (130)
900-1000 μm	90.3% (84)	23.1% (30)
Others	9.7% (9)	76.9% (100)

IV. EXPERIMENTAL RESULTS AND DISCUSSIONS

A. Worm Culture and Microfluidic Device Preparation

We used wild type worm strain in the sorting experiments. Three batches of worms fed with OP50 *E. coli* were separately cultured in an incubator at 20°C for 45, 50 and 55 hours, allowing them to reach L4, young adult and adult stages, respectively. They were then picked out of their culture plates, mixed together, and washed by M9 solution for sorting. Before each experiment, the bottom flow channels were filled with M9 solution without any air bubble. The washed mixture of worms at L4, young adult and adult stages were loaded into the worm loading chamber for sorting experiments. We demonstrated sorting of worms at three consecutive developmental states (L4, young adult and adult), because in real biological experiments the size-based phenotypes of *C. elegans* usually have size difference of approximately 1-2 developmental stages.

B. Automatic Sorting of Young Adult Worms

The mixture of L4, young adult, and adult worms ranges in size from 600 μm to 1300 μm. We aimed to sort out young adult worms and chose a typical size range of $900-1000$ μm for them. Fig. 8 shows the screen shots of the observation chamber and the worm at the three operation steps, and Video S1 illustrates the real-time sorting operations without human intervention. We performed experiments on sorting five

TABLE IV
THE COMPARISON OF MICROFLUIDIC *C. ELEGANS* SORTING DEVICES BASED ON THE WORM SIZE AND/OR DEVELOPMENTAL STAGE

References	Sorting mechanism	Reported speed	Sorting conducted	Size measurement
[22]	electrotactic response	78 worms/min;>79%	383	No
[18]	electrotaxis response	4.3±1.0 worms/min;95±8%		No
[19]	electrotaxis response	56 worms/min;82.62%–89.31%	~200	No
[24]	pillar arrays	200 worms/min; >90%		No
[25]	pillar arrays	>100 worms/min; >85%	>2000	No
[26]	microchannels with tunable cross-section areas	3.5 worms/sec;100%		No
our system	vision-based size measurement	5.8 sec/worm;90.3%	319	Yes

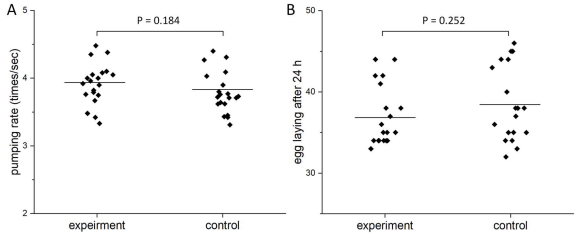

Fig. 9. Survival testing results of the sorted worms. A, B: Values (n = 20) of the worm pumping rate and the progeny number, respectively.

batches of worms with a total number of 319 worms, and statistics of the sorting results are summarized in Table II. In total, 279 times of sorting were conducted, among which 252 times of sorting was successful (meaning that the body size measurement and sorting were both successful on a single worm), 23 times of sorting were detected to be multi-worm loading, and 4 times of sorting were detected to be calculation failures. The total time spent on the 252 successful sorts was 1460 s, corresponding to an average sorting speed of 10.4 worms per minutes (5.8 s per worm). The sorting success rate, which is defined as the ratio of the number of the successfully sorted worms to the total sorting times, was calculated to be 90.3%. The calculation failures occurred when a single worm had coiling behavior, or when multiple worms were loaded simultaneously with their bodies contacted each other throughout entire worm trapping period (1 s) for body size measurement. One can see that the number of multi-worm loading cases is significantly higher than that of calculation failures.

Table IV compares our design with previously reported microfluidic worm sorting methods based on the worm size or developmental stage. One can see that, although our method does not provide the highest sorting speed and the highest success rate, it is the only method capable of simultaneous size measurement and size-based sorting of single worms. The function of worm size measurement "on the fly" could benefit studies requiring accurate size-based sorting with size statistics of the sorted population.

C. Size Validation of the Sorted Worms

To further evaluate the effectiveness of the worm sorting system, we collected the sorted young adult worms and the 'waste' worms from the device's collection and waste outlets, respectively, and measured their lengths on two separate agar

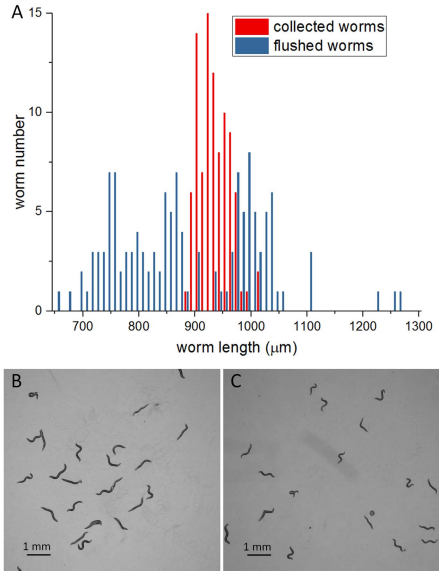

Fig. 10. Post-sorting measurement. A: Body length measurement data of the sorted worms using WormLab. B:, C: Photographs of (B) the sorted worms and (C) the 'waste' worms.

plates using the commercial software WormLab. Fig. 10A shows the body length distributions of the two groups. Fig. 10B and C are the photographs of sorted worms and 'waste' worms. Note only portions of the sorted and 'waste' worms are shown here. From Fig. 10A, one can observe that most of the sorted worms as young adults have body lengths within the range of 900−1000 μm, and nine worms have body lengths (measured by WormLab) slightly smaller than 900 μm or slightly larger than 1000 μm were also collected as young adults. This is due to the measurement inaccuracy (10.8 μm) of the worm length measurement algorithm. Also, 20 worms collected from the waste outlet also has the body lengths falling into the range of 900 − 1000 μm. These worms the system missed were from the detected cases of multi-worm loading and calculation failure (67 worms in total).

D. Viability Tests

To examine the possible impact on the physiology of the sorted worms, we measured two major developmental parameters (pharyngeal pumping rate and fecundity) of the sorted worms and the corresponding control group. The control group

was cultured under the same condition as that of the sorted group. One hour after the sorting experiment, we transferred 20 hermaphrodite individuals from the sorted worms and 20 from the control group onto new agar plates, the pumping rates of which were measured for comparison (data shown in Fig. 9A). After that, these hermaphrodite worms were further cultured on 40 new NGM plates with one worm in each plate for 24 hours. These hermaphrodite worms laid eggs during this period of time, and the number of eggs on each plate were counted as the fecundity (data shown in Fig. 9B). From Fig. 9, one can see that no significant difference was found on the pharyngeal pumping rate and fecundity of the sorted worms and the control ones, confirming that there was no evidence that our system caused any adverse effect on the development of the sorted worms.

V. Conclusion

We presented a vision-based microfluidic system, consisting of a microfludic device and image processing algorithms, for automated, size-based sorting of *C. elegans*. The microfluidic device is responsible for on-chip loading, trapping, imaging, and sorting of single worms. Customizable image processing algorithms were developed for accurate measurement of the worm body size parameters. Based on the sorting experiments of 319 worms, the system provided an average sorting speed of 10.4 worms per minute (5.8 s/worm) with an operation success rate of 90.3%. Post-sorting size measurements on the sorted worms demonstrated the effectiveness of the system.

Acknowledgment

The authors are grateful to Prof. Michael Hendricks at McGill University for assistance in worm culture and handling.

References

[1] H. M. Ellis and H. R. Horvitz, "Genetic control of programmed cell death in the nematode *C. elegans*," *Cell*, vol. 44, no. 6, pp. 817–829, 1986.

[2] M. D. Bono and C. I. Bargmann, "Natural variation in a neuropeptide y receptor homolog modifies social behavior and food response in *C. elegans*," *Cell*, vol. 94, no. 5, pp. 679–689, 1998.

[3] A. Fire, S. Xu, M. K. Montgomery, S. A. Kostas, S. E. Driver, and C. C. Mello, "Potent and specific genetic interference by double-stranded RNA in *Caenorhabditis elegans*," *Nature*, vol. 391, pp. 806–811, Feb. 1998.

[4] C. A. Wolkow, K. D. Kimura, M.-S. Lee, and G. Ruvkun, "Regulation of *C. elegans* life-span by insulinlike signaling in the nervous system," *Science*, vol. 290, no. 5489, pp. 147–150, 2000.

[5] R. B. Azevedo, P. D. Keightley, C. Laurén-Määttä, L. L. Vassilieva, M. Lynch, and A. M. Leroi, "Spontaneous mutational variation for body size in *Caenorhabditis elegans*," *Genetics*, vol. 162, no. 2, pp. 755–765, 2002.

[6] G. Soete, M. C. Betist, and H. C. Korswagen, "Regulation of *Caenorhabditis elegans* body size and male tail development by the novel gene lon-8," *BMC Develop. Biol.*, vol. 7, no. 1, p. 20, 2007.

[7] C. Savage-Dunn, L. Yu, K. Gill, M. Awan, and T. Fernando, "Non-stringent tissue-source requirements for BMP ligand expression in regulation of body size in *Caenorhabditis elegans*," *Genet. Res.*, vol. 93, no. 6, pp. 427–432, 2011.

[8] T. Hirose, Y. Nakano, Y. Nagamatsu, T. Misumi, H. Ohta, and Y. Ohshima, "Cyclic GMP-dependent protein kinase EGL-4 controls body size and lifespan in *C. elegans*," *Development*, vol. 130, no. 6, pp. 1089–1099, 2003.

[9] J. E. Kammenga *et al.*, "A *Caenorhabditis elegans* wild type defies the temperature-size rule owing to a single nucleotide polymorphism in TRA-3," *PLoS Genet.*, vol. 3, no. 3, p. e34, 2007.

[10] M. Fujiwara, P. Sengupta, and S. L. Mcintire, "Regulation of body size and behavioral state of *C. elegans* by sensory perception and the EGL-4 cGMP-dependent protein kinase," *Neuron*, vol. 36, no. 6, pp. 1091–1102, 2002.

[11] W. Y. Fung, K. F. C. Fat, C. K. S. Eng, and C. K. Lau, "crm-1 facilitates BMP signaling to control body size in *Caenorhabditis elegans*," *Develop. Biol.*, vol. 311, no. 1, pp. 95–105, 2007.

[12] A. San-Miguel and H. Lu, "Microfluidics as a tool for *C. elegans* research," in *WormBook*. Pasadena, CA, USA: WormBook Research Community, 2005. doi: 10.1895wormbook.1.162.1.

[13] N. A. Bakhtina and J. G. Korvink, "Microfluidic laboratories for *C. elegans* enhance fundamental studies in biology," *RSC Adv.*, vol. 4, no. 9, pp. 4691–4709, 2014.

[14] A. Ben-Yakar, N. Chronis, and H. Lu, "Microfluidics for the analysis of behavior, nerve regeneration, and neural cell biology in *C. elegans*," *Current Opinion Neurobiol.*, vol. 19, no. 5, pp. 561–567, 2009.

[15] Q. Wen *et al.*, "Proprioceptive coupling within motor neurons drives *C. elegans* forward locomotion," *Neuron*, vol. 76, no. 4, pp. 750–761, 2012.

[16] R. C. Lagoy and D. R. Albrecht, "Microfluidic devices for behavioral analysis, microscopy, and neuronal imaging in *Caenorhabditis elegans*," in *Proc. Methods Mol. Biol.*, 2015, pp. 159–179.

[17] P. Song, W. Zhang, A. Sobolevski, K. Bernard, S. Hekimi, and X. Liu, "A microfluidic device for efficient chemical testing using *Caenorhabditis elegans*," *Biomed. Microdevices*, vol. 17, no. 2, p. 38, 2015.

[18] B. Han, D. Kim, U. H. Ko, and J. H. Shin, "A sorting strategy for *C. elegans* based on size-dependent motility and electrotaxis in a microstructured channel," *Lab Chip*, vol. 12, no. 20, pp. 4128–4134, 2012.

[19] X. Wang *et al.*, "Highly efficient microfluidic sorting device for synchronizing developmental stages of *C. elegans* based on deflecting electrotaxis," *Lab Chip*, vol. 15, no. 11, pp. 2513–2521, 2015.

[20] P. Song, X. Dong, and X. Liu, "A microfluidic device for automated, high-speed microinjection of *Caenorhabditis elegans*," *Biomicofluidics*, vol. 10, 2016, Art. no. 011912.

[21] J. Yuan, J. Zhou, D. M. Raizen, and H. H. Bau, "High-throughput, motility-based sorter for microswimmers such as *C. elegans*," *Lab Chip*, vol. 15, no. 13, pp. 2790–2798, 2015.

[22] P. Rezai, S. Salam, P. R. Selvaganapathy, and B. P. Gupta, "Electrical sorting of *Caenorhabditis elegans*," *Lab Chip*, vol. 12, no. 10, pp. 1831–1840, 2012.

[23] X. Maniére, F. Lebois, I. Matic, B. Ladoux, J.-M. D. Meglio, and P. Hersen, "Running worms: *C. elegans* self-sorting by electrotaxis," *PLoS ONE*, vol. 6, no. 2, 2011, Art. no. 16637.

[24] X. C. I. Solvas, F. M. Geier, A. M. Leroi, J. G. Bundy, and J. B. Edel, "High-throughput age synchronisation of *Caenorhabditis elegans*," *Chem. Commun.*, vol. 47, no. 35, pp. 9801–9803, 2011.

[25] X. Ai, W. Zhuo, Q. Liang, P. T. McGrath, and H. Lu, "A high-throughput device for size based separation of *C. elegans* developmental stages," *Lab Chip*, vol. 14, no. 10, pp. 1746–1752, 2014.

[26] L. Dong, M. Cornaglia, T. Lehnert, and M. A. M. Gijs, "Versatile size-dependent sorting of *C. elegans* nematodes and embryos using a tunable microfluidic filter structure," *Lab Chip*, vol. 16, no. 3, pp. 574–585, 2016.

[27] C. B. Rohde, F. Zeng, R. Gonzalez-Rubio, M. Angel, and M. F. Yanik, "Microfluidic system for on-chip high-throughput whole-animal sorting and screening at subcellular resolution," *Proc. Nat. Acad. Sci. USA*, vol. 104, no. 35, p. 13891–13895, 2007.

[28] M. M. Crane, K. Chung, and H. Lu, "Computer-enhanced high-throughput genetic screens of *C. elegans* in a microfluidic system," *Lab Chip*, vol. 9, no. 1, pp. 38–40, 2009.

[29] Y. Yan *et al.*, "A continuous-flow *C. elegans* sorting system with integrated optical fiber detection and laminar flow switching," *Lab Chip*, vol. 14, no. 20, pp. 4000–4006, 2014.

[30] K. Chung, M. M. Crane, and H. Lu, "Automated on-chip rapid microscopy, phenotyping and sorting of *C. elegans*," *Nature Methods*, vol. 5, no. 7, pp. 637–643, 2008.

[31] S. So, K. Miyahara, and Y. Ohshima, "Control of body size in *C. elegans* dependent on food and insulin/IGF-1 signal," *Genes Cells*, vol. 16, no. 6, pp. 639–651, 2011.

[32] J. Jung, M. Nakajima, M. Kojima, K. Ooe, and T. Fukuda, "Microchip device for measurement of body volume of *C. elegans* as bioindicator application," *J. Micro-Nano Mechatron.*, vol. 7, nos. 1–3, pp. 3–11, 2012.

[33] N. Otsu, "A threshold selection method from gray-level histograms," *IEEE Trans. Syst., Man, Cybern.*, vol. SMC-9, no. 1, pp. 62–66, 1979.

[34] N. Roussel, C. A. Morton, F. P. Finger, and B. Roysam, "A computational model for *C. elegans* locomotory behavior: Application to multiworm tracking," *IEEE Trans. Biomed. Eng.*, vol. 54, no. 10, pp. 1786–1797, 2007.